# Thermodynamic Analysis of Solid−Solid and Solid−Liquid Equilibria in Binary Systems Composed of *n*-Alkanes: Application to the System Tricosane ($C_{23}H_{48}$) + Pentacosane ($C_{25}H_{52}$)

Fazil Rajabalee,[†] Valérie Métivaud,[†] Denise Mondieig,*[,†] and Yvette Haget[†]

*Centre de Physique Moléculaire Optique et Hertzienne, UMR 5798 au CNRS−Université Bordeaux I, F-33405 Talence Cedex, France*

Harry A. J. Oonk[†]

*Chemical Thermodynamics Group, Faculty of Chemistry and Petrology Group, Faculty of Earth Sciences, Utrecht University, Budapestlaan 4, 3584 CD Utrecht, The Netherlands*

*Received March 26, 1999. Revised Manuscript Received July 2, 1999*

This paper presents the elements needed to carry out thermodynamic assessments of phase equilibria in binary systems of normal alkanes in the range from hexadecane ($C_{16}H_{34}$) to octacosane ($C_{28}H_{58}$) and so for the transition from the ordered mixed solid state to the mixed rotator state: the methodology of the computations and the transition properties of the pure component substances as a function of chain length. The proposed approach is applied to the system tricosane ($C_{23}H_{48}$) + pentacosane ($C_{25}H_{52}$), for which the basic experimental phase diagram data are presented.

## Introduction

The normal alkanes $C_nH_{2n+2}$ (hereafter denoted by $C_n$) are important constituents of petroleum waxes which have a broad utility. For reasons of applicability and also from the point of view of fundamental research, substantial attention has been given—during the past two decades—to pure *n*-alkanes and to mixtures of *n*-alkanes.[1−17] These materials have been studied from many research angles, including crystallography and thermodynamics, the fields of research where the underlying study is situated. In recent years, many authors[1,2,9−13] put forward complex binary phase diagrams of alkanes with multiple phases observed as a function of composition and temperature. Nowadays, it is accepted that no continuous miscibility is observed in binary systems of *n*-alkanes even if the crystal symmetries of the pure components are the same (case of odd−odd and even−even alkane systems). Indeed, experimental binary phase diagrams[1,2,9−13] have shown that no continuous miscibility is observed in the orthorhombic $O_i$ form in the case of odd−odd systems or the $T_p$ form in the case of even−even systems, but instead, several phases are observed as a function of composition (in addition to the $O_i$ and $T_p$ forms) which are stabilized by mixing but are not observed for the pure components. These phases were for a long time not identified from a structural and thermodynamical point of view. Recently, these forms were identified,[10,12] and it was shown that these forms, stabilized by mixing, are those observed in long alkanes as from $C_{25}$. These observations were later confirmed on other binary systems of *n*-alkanes.[11,13]

Some calculated thermodynamic equilibria in binary systems of alkanes have been published[3−7] that concern solid−liquid equilibrium. Attempts to modelize solid−solid equilibria have been undertaken[18,19] without the knowledge of the structure of the solid ordered phases.

[†] All members of the REALM (Réseau Européen sur les ALliages Moléculaires).

* To whom correspondence may be addressed. Telephone 00(33)-556846988; Fax 00(33)556846686; E-mail dmondiei@frbdx11.cribx1.u-bordeaux.fr.

(1) Luth, H.; Nyburg, S. C.; Robinson, P. M.; Scott, H. E. *Mol. Cryst. Liq. Cryst.* **1974**, *27*, 337.
(2) Gerson, A. R.; Nyburg, S. C. *Acta Crystallogr. B* **1994**, *50*, 252.
(3) Espeau, P. European Label Thesis of the University Bordeaux I, France, 1995.
(4) Roblès, L. European Label Thesis of the University Bordeaux I, France, 1995.
(5) Rajabalee, F.; Espeau, P.; Haget, Y. *Mol. Cryst. Liq. Cryst.* **1995**, *269*, 165.
(6) Espeau, P.; Oonk, H. A. J.; van der Linde, P. R.; Alcobe, X.; Haget Y. *J. Chim. Phys.* **1995**, *92*, 747.
(7) Roblès, L.; Espeau, P.; Mondieig, D.; Haget, Y.; Oonk, H. A. J. *Thermochim. Acta* **1996**, *274*, 61.
(8) Poirier, B. Thesis of the University Bordeaux I, France, 1996.
(9) Dirand, M.; Achour, Z.; Jouti, B.; Sabour, A.; Gachon, J. C. *Mol. Cryst. Liq. Cryst.* **1996**, *275*, 293.
(10) Rajabalee, F. European Label Thesis of the University Bordeaux I, France, 1998.
(11) Métivaud, V.; Rajabalee, F.; Mondieig, D.; Haget Y.; Cuevas-Diarte, M. A. *Chem. Mater.* **1999**, *11*, 117.
(12) Rajabalee, F.; Métivaud, V.; Mondieig, D.; Haget, Y.; Cuevas-Diarte, M. A. *J. Mater. Res.* **1999**, *14* (6), 2644.
(13) Métivaud, V.; Rajabalee, F.; Cuevas-Diarte, M. A.; Calvet, T.; Mondieig, D.; Haget, Y. *Anal. Quim.*, in press.
(14) Haget, Y.; Mondieig, D.; Cuevas-Diarte, M. A. CNRS Patent FR91/08695 and foreign copending patent applications.
(15) Mondieig, D.; Haget, Y.; Labrador, M.; Cuevas-Diarte, M. A.; Van der Linde, P. R.; Oonk, H. A. J. *Mater. Res. Bull.* **1991**, *26*, 1091.
(16) Espeau, P.; Mondieig, D.; Haget, Y.; Cuevas-Diarte, M. A. *Packag. Technol. Sci.* **1997**, *10*, 253.
(17) Mondieig, D.; Marbeuf, A.; Robles, L.; Espeau, P.; Poirier, B.; Haget, Y.; Calvet-Pallas, T.; Cuevas-Diarte, M. A. *High Temp.—High Pressures* **1997**, *29*, 385.

10.1021/cm991039+ CCC: $18.00 
Published on Web 09/23/1999

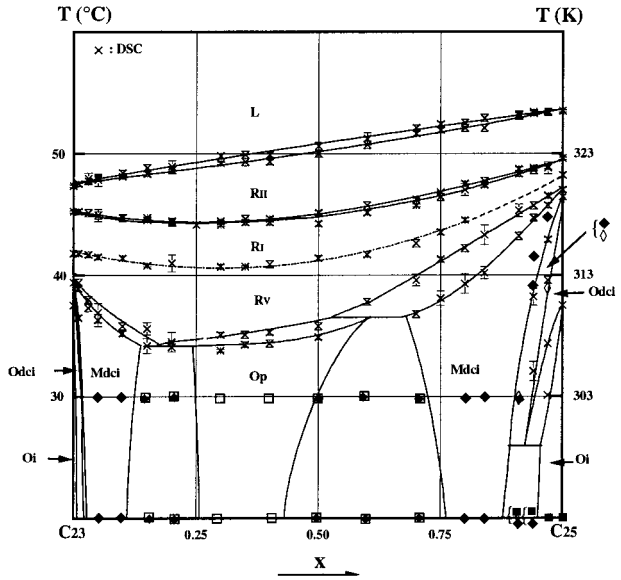


**Figure 1.** Experimental phase diagram $C_{23}$−$C_{25}$.

In a previous paper,[12] we focused on X-ray diffraction studies in binary mixed samples of $C_{23}$ + $C_{25}$, and we gave, for convenience, the experimental phase diagram (without any calorimetric data). We have shown that seven one-phase domains exist at low temperature, and we have been able to characterize all the solid ordered forms observed in the binary phase diagram. These low-temperature phases, newly characterized, lead to new thermodynamic considerations for the modelization of solid−solid and solid−liquid equilibria in binary systems of *n*-alkanes. The information on binary systems is rapidly increasing, and it asks for a uniform thermodynamic approach. It is the aim of the present paper to provide the elements for such a system-independent thermodynamic analysis of phase equilibrium data and to present the results for the system [(1 − *x*)mole of $C_{23}$ + (*x*)mole of $C_{25}$].

As can be observed from Figure 1, the phase diagram for the $C_{23}$ + $C_{25}$ system, the *n*-alkanes have a rich polymorphic nature (which, apart from temperature and pressure, is a function of chain length *n* and the parity of *n*). As a matter of fact, several forms make first their appearance in binary systems and are later on, read for higher values of *n*, also observed for the pure component substances. For example, the form $M_{dci}$ is observed already in the system $C_{16}$ + $C_{17}$,[10] it is not shown by pure $C_{23}$, and it becomes for the first time stable in $C_{25}$. The form $O_p$ in $C_{23}$ + $C_{25}$ is not at all shown by $C_{23}$ and $C_{25}$, $C_{28}$ being the first pure alkane for which it is observed and only so under metastable conditions.[8,10]

A transparent thermodynamic analysis of the various equilibria in a system like $C_{23}$ + $C_{25}$ can be constructed by considering the equilibria one after the other. Starting with the transition from liquid to the rotator form $R_{II}$, one can derive—from the [L + $R_{II}$] loop characteristics and the transition (melting) properties of $C_{23}$ and $C_{25}$—the excess Gibbs energy difference between the liquid and $R_{II}$. Knowing that the liquid mixtures are virtually ideal, one can assign the complete difference to the phase $R_{II}$. As a next step, the [$R_{II}$ + $R_I$] loop and the transition $R_{II}$ → $R_I$ properties of the pure components can be used to calculate the very small excess Gibbs energy difference between $R_I$ and $R_{II}$. From that difference and the value of $R_{II}$ (derived from the analysis of the [L + $R_{II}$] loop) the excess Gibbs energy of $R_I$ can be calculated and so on until the change from $R_V$ to $O_p$. In the case of the [$R_V$ + $O_p$] domain, the $R_V$ → $O_p$ transition properties of the pure components are needed. Reliable estimates of these properties are given in this paper; they originate from a comparative study of the same transition in other binary *n*-alkane systems.

In the remainder of this paper, first an account is given of the thermodynamic formalism, and the estimates of the pure component transition data are presented. Thereafter, details are given of the various transitions in the system $C_{23}$ + $C_{25}$. Finally, the outcome of the thermodynamic analysis is presented.

## Experimental Section

**Thermodynamic Analysis.** In the case of the various equilibria to be considered, two Gibbs energy functions are needed: one for the low-temperature form, denoted by α, and one for the high-temperature form, *β*. As a function of the variables *T* (temperature) and *x* (mole fraction of component B in the system [(1 − *x*)mole of A + (*x*)mole of B], the Gibbs energy functions generally are given as

$$G^{\beta}(T,x) = (1-x)G_A^{*,\beta}(T) + xG_B^{*,\beta}(T) + RT\{(1-x)\ln(1-x) + x\ln x\} + G^{E,\beta}(T,x) \quad (1)$$

$$G^{\alpha}(T,x) = (1-x)G_A^{*,\alpha}(T) + xG_B^{*,\alpha}(T) + RT\{(1-x)\ln(1-x) + x\ln x\} + G^{E,\alpha}(T,x) \quad (2)$$

where *R* is the gas constant ($R$ = 8.314 51 J $K^{-1}$ $mol^{-1}$) and the superscript * refers to the pure component. $G^E$ is for excess Gibbs energy, the deviation from ideal mixing behavior.

Subtraction of eq 2 from eq 1 gives

$$\Delta_{\alpha}^{\beta}G(x,T) = (1-x)\Delta_{\alpha}^{\beta}G_A^*(T) + x\Delta_{\alpha}^{\beta}G_B^*(T) + \Delta_{\alpha}^{\beta}G^E(x,T) \quad (3)$$

The solution of the equation

$$\Delta_{\alpha}^{\beta}G(x,T) = 0 \quad (4)$$

corresponds to a curve in the *T*−*x* plane, the equal *G* curve (EGC)[20] at which the Gibbs energies of α and *β* are equal. In the phase diagram, the EGC is running between the two (α-equilibrium and *β*-equilibrium) curves; it means that its position can be indicated in an accurate manner, the more so the narrower the [α + *β*] loop.

The other way round, as follows from eqs 3 and 4, the estimated position of the EGC in the *T*−*x* plane enables us to calculate the excess Gibbs energy difference $\Delta_{\alpha}^{\beta}G^E$. To that end, the pure component properties $\Delta_{\alpha}^{\beta}G_A^*$ and $\Delta_{\alpha}^{\beta}G_B^*$ have to be known. In our case, where the equilibria take place in a small interval on the temperature scale, $\Delta_{\alpha}^{\beta}G_A^*$ and $\Delta_{\alpha}^{\beta}G_B^*$ can be taken as linear functions of temperature

$$\Delta_{\alpha}^{\beta}G_i^*(T) = \Delta_{\alpha}^{\beta}H_i^* - T\Delta_{\alpha}^{\beta}S_i^*, \quad i = A, B \quad (5)$$

which means that the changes of the transition enthalpy $\Delta_{\alpha}^{\beta}H_i^*$ and the transition entropy $\Delta_{\alpha}^{\beta}S_i^*$ with temperature are ignored. (In other words, the transition heat capacities are neglected.) At the α → *β* transition temperature $\Delta_{\alpha}^{\beta}G_i^*$ is equal to zero, which means that $\Delta_{\alpha}^{\beta}H_i^*$ and $\Delta_{\alpha}^{\beta}S_i^*$ are

(18) Sabour, A. Thesis of the I. P. L., Nancy, France, 1994.
(19) Provost, E. Thesis of the I. P. L., Nancy, France, 1997.
(20) Oonk, H. A. J. *Phase Theory*; Elsevier Sci. Publ.: Amsterdam, 1981.

related as

$$\Delta_\alpha^\beta H_i^* - T_i^{\alpha\rightarrow\beta}\,\Delta_\alpha^\beta S_i^* = 0 \qquad (6)$$

In practice, the pure component properties $T_i^{\alpha\rightarrow\beta}$ and $\Delta_\alpha^\beta S_i^*$ along with the phase diagram data are used as input for the computer program LIQFIT.[21] In this program, the computations are directed by the EGC, until maximum agreement between either experimental and calculated α-equilibrium or experimental and calculated $\beta$-equilibrium curve. The output of LIQFIT is the optimized [α + $\beta$] phase equilibrium diagram along with the calculated excess Gibbs energy difference $\Delta_\alpha^\beta G^E$ in a prescribed mathematical form. In the case of the alkane equilibria, the temperature range of the phenomena is rather small, and for that reason we normally express the difference function (a Redlich−Kister second-order polynomial function) as

$$\Delta_\alpha^\beta G^E(x,T) = \Delta_\alpha^\beta G^E(x) = x(1-x)[\Delta_\alpha^\beta G_1 + (1-2x)\Delta_\alpha^\beta G_2] \qquad (7)$$

It means that the values of the adjusted parameters $\Delta_\alpha^\beta G_1$ and $\Delta_\alpha^\beta G_2$ are valid for the mean temperature of the α → $\beta$ transition. (It may be remarked that the calculated $\Delta G^E$ can be combined with the experimental $\Delta H^E$ function, when available, to yield the function $\Delta S^E$.[22,23])

**Pure Component Properties.** In experimental practice, phase diagram data are collected by means of (micro)calorimetry, which at the same time yields transition enthalpies. The latter, in the case of the alkanes and for a given α → $\beta$ transition, change with chain length in a gradual manner. It means that, even if an individual value is less accurate than would be desired, the whole collection of data as a function of chain length will give a precise record of the property and read the transition enthalpy and on the same lines of reasoning also transition temperatures. Having stated this, we present in this paper new information on the transitions from the ordered forms to the rotator form R. Since the energy effects for the R → R transition are very weak if not zero, we have decided to ignore these effects in the thermodynamic analyses of the transition from ordered form to rotator form. In other words, from now we will consider a unique form R, instead of $R_V$, $R_I$, and $R_{III}$.

*(a) Transition Temperatures.* In the case of the transition from $M_{dci}$ to R ($R_V$ for $C_{25}$, $R_{III}$ for $C_{27}$ and $C_{29}$), there is direct information for $C_{25}$, $C_{27}$, and $C_{29}$: for these alkanes, the $M_{dci}$ form makes a stable appearance. The transition temperature for $C_{29}$ has been given by Maroncelli et al.[24] In addition to the three values, we obtained values for $C_{17}$, $C_{19}$, $C_{21}$, and $C_{23}$ by means of extrapolation of transition temperatures in several binary systems (odd−odd, even−odd, and odd−even[34]). As an example, from Figure 1, it is clear that for $C_{23}$ a reliable value of the transition temperature can be obtained by extrapolation to $x = 0$ of the two [$M_{dci}$ + R] equilibrium curves. At the same time, it is obvious that for this system the extrapolation of the equilibrium curves for [$O_p$ + R] to $x = 0$ and $x = 1$ would be more troublesome. As a matter of fact, the $O_p$ → R transition temperatures can be obtained in a reliable manner from binary systems involving at least one even component, although for none of the even alkanes studied from $C_8$ to $C_{28}$ does the form $O_p$ make a stable appearance. Under metastable conditions it appears for the even alkanes with $n \geq 28$;[8] the [$O_p$] domains

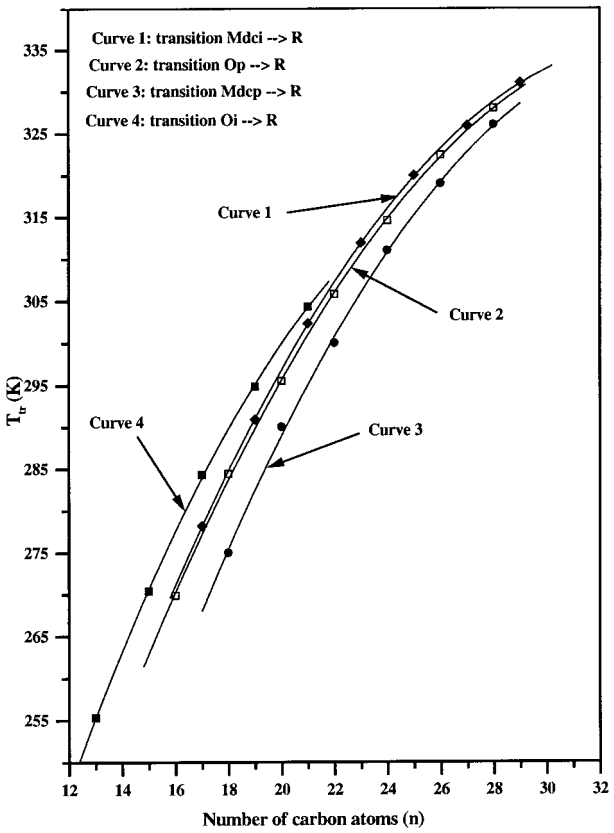


**Figure 2.** Variation of the temperature phase transitions with chain length ($n$).

in the phase diagrams are at the side(s) of the even component-(s)[10,11,13] which allows a reliable extrapolation to the axis $x$ = 0 and for the axis $x = 1$. For the pure alkanes, as a result of these operations, the transition temperatures from $M_{dci}$ to R and from $O_p$ to R are given by the formulas

$$T_{tr}^{M_{dci}\rightarrow R}\,(K) = 103.1 + 13.754n - 0.20327n^2 \qquad (8)$$

$$T_{tr}^{O_p\rightarrow R}\,(K) = 107.6 + 13.220n - 0.19107n^2 \qquad (9)$$

See also Figure 2.

In addition to $M_{dci}$ and $O_p$, there are two more solid forms to be considered: $M_{dcp}$ (which do not appear in Figure 1) and $O_i$. The form $M_{dcp}$ invariably appears in the central part of even−even phase diagrams, and its stability field is growing from $C_{14} + C_{16}$ to $C_{26} + C_{28}$.[10] The first of these facts implies that any extrapolation to $x$ =0 and $x = 1$ will be somewhat hazardous. Being aware of this, we made for the completely determined systems $C_{18} + C_{20}$, $C_{22} + C_{24}$, and $C_{26} + C_{28}$ a series of calculations of the [$M_{dcp}$ + $O_p$] equilibrium, by varying the values of the pure component transition temperatures. The result of this exercise, which at any rate does not violate the experimental results obtained for the other equilibria in the systems, is represented by the formula

$$T_{tr}^{M_{dcp}\rightarrow R}\,(K) = 76.7 + 14.900n - 0.21429n^2 \qquad (10)$$

The individual points are shown in Figure 2 where eq 10 is represented by curve 3. The next form to be considered is the form $O_i$. Unlike $M_{dcp}$, it is found in the vicinity of the pure components (and invariably so for the odd alkanes). The transition temperatures are shown in figure, and the curve through the individual points, curve 4, is represented by the formula

$$T_{tr}^{O_i\rightarrow R}\,(K) = 104.5 + 14.984n - 0.26071n^2 \qquad (11)$$

(21) Jacobs, M. H. G.; Oonk, H. A. J. LIQFIT, a computer program for the thermodynamic assessment of vaporus, liquidus, solidus curves in TX phase diagrams (version 1.2), Chemical Thermodynamics Group, Utrecht University, 1989.

(22) Mondieig, D.; Espeau, P.; Roblès, L.; Haget, Y.; Oonk, H. A. J.; Cuevas-Diarte, M. A. *J. Chem. Soc., Faraday Trans.* **1997**, *93* (18), 3343.

(23) Oonk, H. A. J.; Mondieig, D.; Haget, Y.; Cuevas-Diarte, M. A. *J. Chem. Phys.* **1998**, *108* (2), 715.

(24) Maroncelli, M.; Qi, S. P.; Strauss, H. L.; Snyder, R. G. *J. Phys. Chem.* **1982**, *104*, 6237.

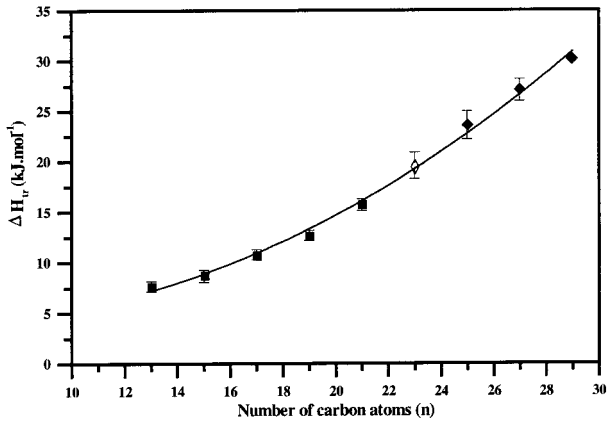


**Figure 3.** Variation of the enthalpy of phase transition with chain length ($n$).

*(b) Transition Enthalpies.* The enthalpy effect of the transition from the ordered form $O_i$ can be measured for the odd alkanes from $C_{13}$ up to $C_{21}$. For the transition from $M_{dci}$ to R, the effect can be measured for $C_{25}$, $C_{27}$, and $C_{29}$. The experimental data are shown in Figure 3, which also includes the enthalpy of transition for $C_{23}$ involving the $O_{dci}$ form. The $O_{dci}$ form, which has not been mentioned hitherto, plays a minor role, at least in the thermodynamic computations, to be presented.

As follows from Figure 3, the nine data points line up in a clear manner: in terms of transition enthalpy, there is no reason to make a distinction between $O_i$, $O_{dci}$, and $M_{dci}$ (apart, of course, from the influence of chain length). The curve drawn through the points is given by the formula

$$\Delta H_{tr}\ (\mathrm{J\ mol^{-1}}) = 5441.8 - 462.273n + 46.18507n^2 \quad (12)$$

For the transition from the forms $O_p$ and $M_{dcp}$ to the rotator form, there are no data involving pure alkanes. Because the solid forms $O_i$, $O_{dci}$, $M_{dci}$, $O_p$, and $M_{dcp}$ are quite similar from a structural point of view, we will adopt the hypothesis that the transitions from $O_p$ and $M_{dcp}$ to R will also be accompanied by a heat effect given by eq 12.

**The System $C_{23}$ + $C_{25}$: Experimental Data.** *(a) Pure Components.* Tricosane and pentacosane were purchased from Fluka and Aldrich, respectively. Their purity grades are 99.3% for $C_{23}$ and 99.1% for $C_{25}$ as determined by gas chromatography and mass spectroscopy. Binary mixed samples were prepared according to the "melting-quenching" method.[4]

$C_{23}$ and $C_{25}$ show a rich polymorphic behavior,[12,25] and with temperature, the following phase transition sequences are observed (the dashed arrows are used for second-order transitions):

$C_{23}$: $O_i \rightarrow O_{dci} \longrightarrow R_V \dashrightarrow R_I \rightarrow R_{II} \rightarrow$ Liquid

$C_{25}$: $O_i \rightarrow O_{dci} \rightarrow M_{dci} \longrightarrow R_V \dashrightarrow R_I \rightarrow R_{II} \rightarrow$ Liquid

Low temperature domain (Ordered crystalline forms) — High temperature domain (Rotator and Liquid forms)

$O_i$ is orthorhombic ($P_{cam}$, $Z = 4$[26]); $O_{dci}$ ($P_{nam}$, $Z = 4$[10,12,27]) is also orthorhombic. (The $O_i \rightarrow O_{dci}$ transition is sometimes referred to as the $\delta$-transition.[28]) $M_{dci}$ is monoclinic ($A_a$, $Z = 4$[29]).The $R_V$ form is monoclinic which can be seen as an inclined version of the $R_I$ form ($Fmmm$, $Z = 4$[29]), and the rotator $R_{II}$ form is hexagonal ($R\bar{3}m$, $Z = 3$). All the rotator forms are well described by Sirota et al.[30,31]

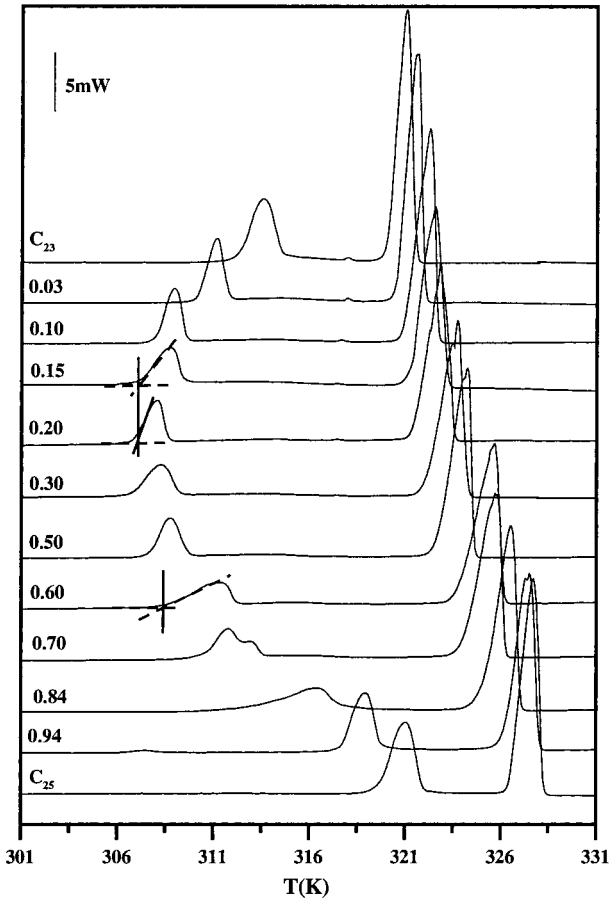


**Figure 4.** Examples of DSC curves as a function of molar fraction in $C_{25}$.

*(b) Experimental Techniques.* The calorimetric measurements were performed using a Perkin-Elmer DSC-7 operating in the liquid nitrogen subambient mode. Details about the conditions adopted are given in our previous paper,[12] and the analysis method of the DSC curves is described elsewhere.[32−33]

X-ray diffraction spectra were recorded using a Siemens D500 vertical powder diffractometer which works in the reflection mode and a Guinier-Simon camera for continuous temperature recording and operating in the transmission mode. In both cases, copper K$\alpha_1$ radiation ($\lambda = 1.5406$ Å) was used. The results of the analyses with the D500 diffractometer were given in our previous paper[12] and are therefore not reported here.

## Results

**Calorimetric Data and Phase Diagram.** Nineteen binary mixed samples were studied by DSC. Figure 4

(25) Robles, L.; Mondieig, D.; Haget, Y.; Cuevas-Diarte, M. A. *J. Chim. Phys* **1998**, *95*, 92.
(26) Smith, A. E. *J. Chem. Phys.* **1953**, *21*, 2229.
(27) Nozaki, K.; Higashitani, N.; Yamamoto, T.; Hara, T. *J. Chem. Phys.* **1995**, *103* (13), 5762.
(28) Snyder, R. G.; Maroncelli, M.; Qi, S. P.; Strauss, H. L. *Science* **1981**, *214*, 188.
(29) Ungar, G. *J. Phys. Chem.* **1983**, *87*, 689.
(30) Sirota, E. B.; King Jr., H. E.; Singer, D. M.; Shao, H. H. *J. Chem. Phys.* **1993**, *98* (7), 5809.
(31) Sirota, E. B.; King Jr., H. E.; Shao, H. H.; Singer, D. M. *J. Phys. Chem.* **1995**, *99*, 798.
(32) Courchinoux, R.; Chanh, N. B.; Haget, Y.; Tauler, E.; Cuevas-Diarte, M. A. *Thermochim. Acta* **1988**, *128*, 45.
(33) Courchinoux, R.; Chanh, N. B.; Haget, Y.; Calvet, T.; Estop, E.; Cuevas-Diarte, M. A. *J. Chim. Phys.* **1989**, *86* (3), 561.
(34) Odd and even stand for components with an odd number and an even number of carbon atoms, respectively.
(35) We have shown[12] that the [$O_p$] form has an orthorhombic structure ($Pca2_1$, $Z = 4$).

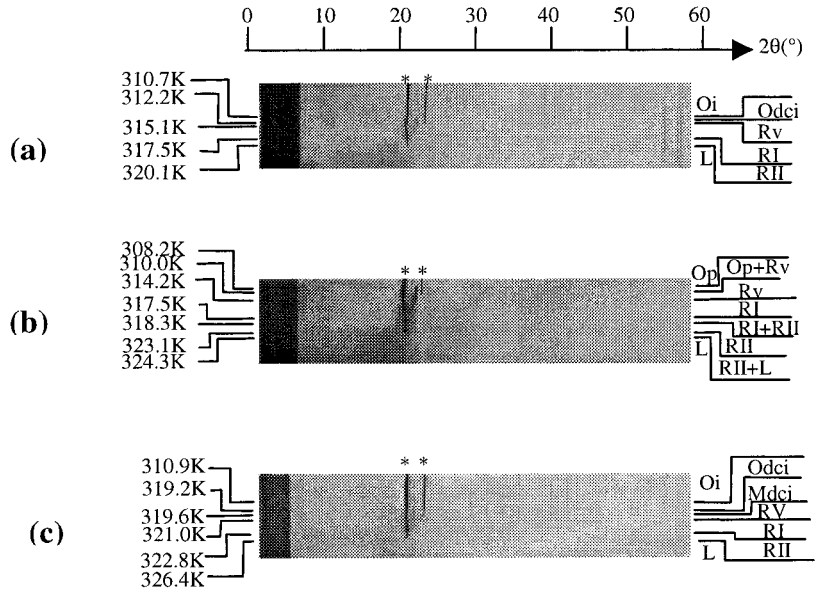


**Figure 5.** Guinier−Simon photographs of the pure components $C_{23}$ **(a)** and $C_{25}$ **(c)** and of the mixed sample $(0.5)C_{23} + (0.5)C_{25}$ **(b).** The two reflections marked by an asterisk correspond to the 110 and 020 lines in the low-temperature region and are indexed as 111 and 020 in the $R_I$ and $R_V$ phases. These two lines join to one single reflection 010 in the $R_{II}$ phase.

illustrates some examples of the DSC curves of the binary system. The vertical lines show the location of the invariant equilibria (a eutectoid and a peritectoid) around $x \approx 0.20$ and $x \approx 0.60$, respectively. The melting temperatures of the mixed samples increase with composition, and the melting enthalpies are higher than any solid−solid transition enthalpy. The melting of the mixed samples takes place within 1.5 K.

**The "High-Temperature" Phase Region: The [$R_{II}$ + Liquid] and [$R_I$ + $R_{II}$] Domains.** At "high temperature", $C_{23}$ and $C_{25}$ are isomorphous, and complete miscibility is observed in the $R_{II}$, $R_I$, and $R_V$ forms. Indeed, the Guinier−Simon photographs of the two components and that of the mixed sample $(0.5)C_{23} + (0.5)C_{25}$ (see Figure 5) show that their structural behaviors as a function of temperature (at high temperature) are identical. The $R_{II}$ phase is characterized by a single intense reflection at around $2\theta \approx 20°$ and the $R_I$ form by two reflections around the same angular position, the two lines 111 and 020 approaching each other. (This is due to the thermal expansion of the *a* and *b* cell parameters with temperature, the ratio *a*/*b* tending toward $\sqrt{3}$; when this value is reached, the hexagonal $R_{II}$ form appears.) The $R_V$ form is difficult to observe in Figure 2, but X-ray diffraction[12] and DSC analyses have confirmed its presence (Figure 6).

The thermoenergetic data for the rotator ($R_I$) → rotator ($R_{II}$) and the melting are given in Table 1 as well as the temperature of the second-order phase transition $R_V \rightarrow R_I$. Both $R_V \rightarrow R_I$ and $R_I \rightarrow R_{II}$ phase transitions show a minimum in temperature around $x \approx 0.25$. This particularity is also observed in other binary systems.[9,11] The enthalpies of melting are very high (around 54 kJ mol$^{-1}$) with respect to those of the $R_I \rightarrow R_{II}$ transition (inferior to 350 J mol$^{-1}$).

**The "Low-Temperature" Phase Region: The [$O_i$ + $O_{dci}$], [$O_{dci}$ + $M_{dci}$], [$M_{dci}$ + $R_I$], and [$O_p$ + $R_I$] Domains.** A zoom of the phase diagram in the compositional region $0.00 \leq x \leq 0.05$ and in the temperature region $279 \leq T$ (K) $\leq 319$ is given in Figure 7. Because

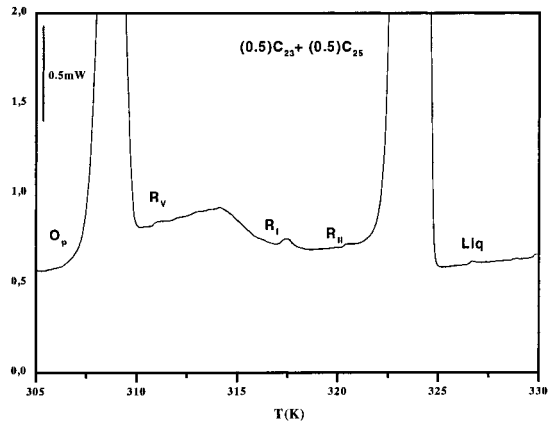


**Figure 6.** DSC thermogram of the mixed sample $(0.5)C_{23} + (0.5)C_{25}$ with rise of temperature from 305 to 330 K.

of the very weak enthalpy effects of the $O_i \rightarrow O_{dci}$ and $O_{dci} \rightarrow M_{dci}$ transitions, it is difficult to obtain the temperatures of phase transitions by DSC measurements only. X-ray diffraction measurements (D500) have enabled us to draw the [ordered solid + ordered solid] loops shown in Figure 7. For example, with a rise in temperature, the structure of the mixed sample $x = 0.01$ is orthorhombic $O_i$ at 279 K, orthorhombic $O_{dci}$ at 307 K, and monoclinic $M_{dci}$ at 311 K. The mixed sample is biphasic at 291 K. The facts that the [$O_{dci}$ + $M_{dci}$] and [$M_{dci}$ + $R_V$] loops are observed and that the component $C_{23}$ does not show the $O_{dci} \rightarrow M_{dci}$ phase transition undoubtedly yield a peritectoïd near $C_{23}$.

The thermoenergetic transition data are reported in Tables 2 and 3 for the ordered solid ($\Phi_{ord}$) → rotator transition and for the $\Phi_{ord} \rightarrow \Phi_{ord}$ transition, respectively. In Table 2, the phase transition enthalpies for the mixed samples are around 12 kJ mol$^{-1}$, about 4 times less than those of the melting. A significant drop in the values of this thermodynamic quantity is observed when compared with those of the components $C_{23}$ and $C_{25}$. Like for the $R_V \rightarrow R_I$ and the $R_I \rightarrow R_{II}$ transitions, a minimum temperature of transition is observed around $x \approx 0.25$. In Table 3, the enthalpy

**Table 1. High-Temperature Thermoenergetic Data ($T$ in K, $\Delta H_{tr}$ in J mol$^{-1}$ and $\Delta H_f$ in kJ mol$^{-1}$)[a]**

| $x$ in $C_{25}$ | transition $R_V \rightarrow R_I$ | transition $R_I \rightarrow R_{II}$ | | | melting | | |
|---|---|---|---|---|---|---|---|
| | | $T_{solvi}$ | $T_{solvs}$ | $\Delta H_{tr}$ | $T_{sol}$ | $T_{liq}$ | $\Delta H_f$ |
| $C_{23}$ | 314.8 ± 0.1 | 317.9 ± 0.1 | | 320 ± 11 | 320.3 ± 0.1 | | 52.6 ± 1.3 |
| 0.01 | 314.8 ± 0.2 | 318.2 ± 0.2 | 318.2 ± 0.2 | 156 ± 6 | 320.5 ± 0.1 | 320.5 ± 0.2 | 52.2 ± 1.1 |
| 0.03 | 314.7 ± 0.2 | 318.1 ± 0.3 | 318.1 ± 0.3 | 147 ± 32 | 320.7 ± 0.2 | 320.9 ± 0.5 | 52.2 ± 1.3 |
| 0.05 | 314.5 ± 0.2 | 317.9 ± 0.3 | 317.9 ± 0.5 | 137 ± 10 | 320.8 ± 0.5 | 321.0 ± 0.2 | 51.8 ± 1.3 |
| 0.10 | 314.4 ± 0.2 | 317.7 ± 0.2 | 317.7 ± 0.3 | 124 ± 16 | 321.1 ± 0.2 | 321.4 ± 0.2 | 52.2 ± 1.1 |
| 0.15 | 313.8 ± 0.1 | 317.5 ± 0.1 | 317.7 ± 0.1 | 89 ± 3 | 321.3 ± 0.2 | 321.8 ± 0.3 | 52.0 ± 1.3 |
| 0.20 | 314.0 ± 0.5 | 317.3 ± 0.3 | 317.4 ± 0.3 | 96 ± 13 | 321.6 ± 0.3 | 321.9 ± 0.5 | 52.6 ± 1.3 |
| 0.30 | 313.7 ± 0.2 | 317.1 ± 0.1 | 317.4 ± 0.1 | 50 ± 3 | 322.2 ± 0.1 | 322.8 ± 0.2 | 52.3 ± 1.7 |
| 0.35 | 313.7 ± 0.1 | 317.3 ± 0.2 | 317.6 ± 0.3 | 70 ± 17 | 322.5 ± 0.3 | 322.9 ± 0.3 | 53.2 ± 1.5 |
| 0.40 | 313.9 ± 0.3 | 317.3 ± 0.2 | 317.6 ± 0.2 | 64 ± 13 | 322.7 ± 0.2 | 323.4 ± 0.2 | 53.4 ± 1.2 |
| 0.50 | 314.4 ± 0.2 | 317.2 ± 0.2 | 318.1 ± 0.2 | 58 ± 7 | 323.3 ± 0.3 | 323.9 ± 0.3 | 54.2 ± 1.7 |
| 0.60 | 314.7 ± 0.2 | 318.1 ± 0.2 | 318.7 ± 0.3 | 27 ± 6 | 324.2 ± 0.3 | 324.7 ± 0.5 | 54.7 ± 1.5 |
| 0.70 | 315.6 ± 0.3 | 318.7 ± 0.1 | 319.2 ± 0.1 | 21 ± 7 | 324.6 ± 0.2 | 325.1 ± 0.2 | 54.7 ± 2.1 |
| 0.75 | 316.5 ± 0.2 | 319.4 ± 0.3 | 319.8 ± 0.1 | 17 ± 7 | 324.9 ± 0.2 | 325.4 ± 0.2 | 55.6 ± 1.3 |
| 0.80 | 317.5 ± 0.2 | 320.0 ± 0.5 | 320.5 ± 0.2 | 31 ± 17 | 325.1 ± 0.3 | 325.5 ± 0.3 | 55.7 ± 2.2 |
| 0.84 | *a* | 320.4 ± 0.2 | 320.7 ± 0.3 | *a* | 325.3 ± 0.3 | 325.9 ± 0.3 | 56.5 ± 1.5 |
| 0.91 | *a* | 321.3 ± 0.2 | 321.7 ± 0.2 | 35 ± 18 | 326.1 ± 0.3 | 326.2 ± 0.3 | 56.9 ± 1.5 |
| 0.94 | *a* | 321.6 ± 0.3 | 321.8 ± 0.2 | 67 ± 11 | 326.3 ± 0.2 | 326.4 ± 0.2 | 56.8 ± 2.2 |
| 0.97 | *a* | 321.8 ± 0.5 | 321.9 ± 0.2 | 67 ± 11 | 326.4 ± 0.2 | 326.4 ± 0.2 | 57.7 ± 1.4 |
| $C_{25}$ | 321.2 ± 0.1 | 322.6 ± 0.1 | | 350 ± 16 | 326.5 ± 0.1 | | 57.8 ± 1.8 |

[a] In these cases, it was not possible to extract the numerical values from the DSC signals due to overlap.

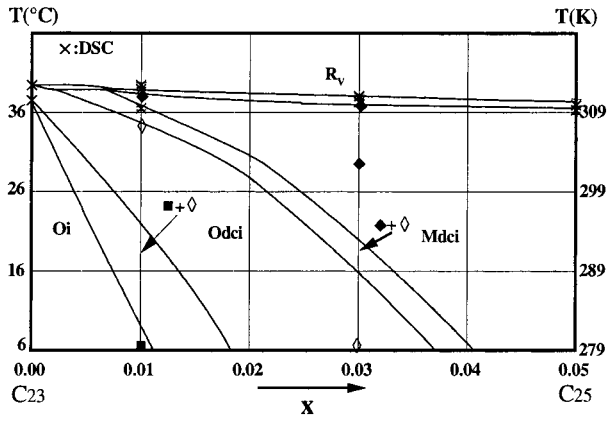


**Figure 7.** Zoom of the phase diagram $C_{23}$–$C_{25}$ in the compositional region $0.00 \leq x \leq 0.05$.

effects are even weaker (negligible for $O_i \rightarrow O_{dci}$ and around 1 J mol$^{-1}$ for the $O_{dci} \rightarrow M_{dci}$). Because of the small value of the enthalpy, the $O_i \rightarrow O_{dci}$ phase transition was not possible to characterize accurately with the DSC apparatus.

The overall analyses of the DSC curves (with the help of the X-ray diffraction measurements[12]) enable us to draw the phase diagram of $C_{23} + C_{25}$ shown in Figure 1.

The phase diagram exhibits no less than (i) 11 one-phase domains—[$O_{i_{C23}}$], [$O_{dci_{C23}}$], [$O_{i_{C25}}$], [$O_{dci_{C25}}$], [$M_{dci_{C25}}$], [$M_{dci_{C25}}$], [$O_p$],[35] [$R_V$], [$R_I$], [$R_{II}$], and [L]; (ii) 2 peritectoids, one close to $C_{23}$ at $T \approx 311.6$ K between $x \approx 0$ and $x \approx 0.01$ and the second at $T \approx 309$ K between $x \approx 0.53$ and $x \approx 0.68$; (iii) 1 eutectoid at $T \approx 307$ K between $x \approx 0.14$ and $x \approx 0.24$; and (iv) a metatectoid at $T \approx 301$ K close to $C_{25}$ between $x \approx 0.90$ and $x \approx 0.96$.

The metatectoid located in the vicinity of $C_{25}$ is not visible in Figure 4. In our previous work,[12] we have shown by X-ray powder diffraction that the mixed sample $x = 0.94$ is biphasic [$O_i + M_{dci}$] at $T = 293$ K and [$O_{dci} + M_{dci}$] at $T = 303$ K, and we suggest that a metatectoid exists at $T \approx 299 \pm 3$ K. The DSC curve of the sample $x = 0.94$ shown in Figure 8 enables us to say that the invariant equilibrium is located at $T \approx 296$ K. The enthalpy effect, being very weak, renders the evaluation of the temperature of the invariant difficult.

**The System $C_{23} + C_{25}$: Thermodynamic Analysis.** The principal aim of the thermodynamic analysis presented in this section is to make a fit of the experimental phase diagram by means of a procedure—LIQFIT—in which the system and form-dependent constants of the excess Gibbs energies act as the parameters to be adjusted. As was mentioned before, the excess Gibbs energy of the liquid mixtures is set at zero, and it implies that there are in total eight parameters to be adjusted. These parameters are $G_1^i$ and $G_2^i$ in the following expression

$$G^{E,i}(x) = x(1-x)\{G_1^i + G_2^i(1-2x)\}, \quad i = R_{II}, R_I, M_{dci}, O_p \quad (13)$$

which implies that only those equilibria are treated that run from left to right in the phase diagram. There are four such equilibria, and they are analyzed one after the other in the phase diagram from top to bottom.

Now focusing on one of these equilibria and denoting the low-temperature form by α and the high-temperature form by $\beta$, we may recall from section 2 that the data allow the calculation of the difference excess Gibbs energy

$$\Delta_\alpha^\beta G^E(x) = x(1-x)\{\Delta_\alpha^\beta G_1 + \Delta_\alpha^\beta G_2(1-2x)\} \quad (14)$$

The computations carried out by LIQFIT are directed by the equal $G$ curve which stands in the following relation to the $\Delta G^E$ function

$$T_{EGC}(x) = T_{ZERO}(x) + \frac{\Delta_\alpha^\beta G^E(x)}{(1-x)\Delta S_A^* + x\Delta S_B^*} \quad (15)$$

where the zero line

$$T_{ZERO}(x) = \frac{(1-x)\Delta_\alpha^\beta H_A^* + x\Delta_\alpha^\beta H_B^*}{(1-x)\Delta_\alpha^\beta S_A^* + x\Delta_\alpha^\beta S_B^*} \quad (16)$$

is a property containing only pure component properties.

**Table 2. Low-Temperature Thermoenergetic Data for the $\Phi_{ord} \rightarrow R_V$ Phase Transitions ($T$ in K and $\Delta H_{tr}$ in kJ mol$^{-1}$)**

| | solid ordered phase transitions ($M_{dci}$, $O_p$) → rotator $R_V$ | | | | | |
|---|---|---|---|---|---|---|
| $x$ in $C_{25}$ | $T_{solvi}$ | $T_P$ | $T_E$ | $T_{P'}$ | $T_{solvs}$ | $\Delta H_{tr}$ |
| $C_{23}$ | | | | | | |
| 0.01 | 311.9 ± 0.2 | | | | 312.4 ± 0.3 | 17.1 ± 0.9 |
| 0.03 | | 310.3 ± 0.3 | | | 311.0 ± 0.3 | 14.1 ± 0.7 |
| 0.05 | 309.3 ± 0.5 | | | | 309.9 ± 0.7 | 13.2 ± 1.0 |
| 0.10 | 308.2 ± 0.2 | | | | 308.8 ± 0.3 | 12.3 ± 0.3 |
| 0.15 | | | 307.2 ± 0.6 | | 308.6 ± 0.5 | 12.1 ± 0.7 |
| 0.20 | | | 307.1 ± 0.5 | | 307.5 ± 0.6 | 11.3 ± 0.5 |
| 0.30 | 306.8 ± 0.1 | | | | 308.1 ± 0.2 | 11.3 ± 0.5 |
| 0.35 | 307.3 ± 0.2 | | | | 308.1 ± 0.3 | 12.1 ± 0.4 |
| 0.40 | 307.4 ± 0.3 | | | | 308.1 ± 0.2 | 12.1 ± 0.4 |
| 0.50 | 307.9 ± 0.2 | | | | 308.8 ± 0.3 | 11.9 ± 1.1 |
| 0.60 | | | | 308.8 ± 0.2 | 311.0 ± 0.3 | 13.4 ± 0.5 |
| 0.70 | 309.8 ± 0.3 | | | | 312.6 ± 0.5 | 12.2 ± 0.8 |
| 0.75 | 311.1 ± 0.1 | | | | 314.3 ± 0.2 | 15.5 ± 0.5 |
| 0.80 | 312.3 ± 0.2 | | | | 315.2 ± 0.3 | 16.8 ± 1.0 |
| 0.84 | 313.2 ± 0.5 | | | | 317.3 ± 0.7 | 17.6 ± 1.8 |
| 0.91 | 316.2 ± 0.3 | | | | 318.3 ± 0.5 | 18.4 ± 1.2 |
| 0.94 | 317.7 ± 0.3 | | | | 318.7 ± 0.3 | 19.8 ± 2.2 |
| 0.97 | 318.7 ± 0.2 | | | | 319.5 ± 0.2 | 22.4 ± 0.9 |
| $C_{25}$ | 320.0 ± 0.2 | | | | | 23.6 ± 1.4 |

**Table 3. Low-Temperature Thermoenergetic Data for the $\Phi_{ord} \rightarrow \Phi_{ord}$ Phase Transitions ($T$ in K and $\Delta H_{tr}$ in J mol$^{-1}$)**

| | solid ordered → solid ordered phase transitions | | | | | |
|---|---|---|---|---|---|---|
| | $O_i \rightarrow O_{dci}$ phase transition | | | $O_{dci} \rightarrow M_{dci}$ phase transition | | |
| $x$ in $C_{25}$ | $T_{solvi}$ | $T_{solvs}$ | $\Delta H_{tr}$ | $T_{solvi}$ | $T_{solvs}$ | $\Delta H_{tr}$ |
| $C_{23}$ | 310.5 | | <0.3 | | | |
| 0.01 | | | | 309.5 ± 0.7 | 311.0[a] | |
| 0.03 | | | | 283.1 ± 2.2 | 296.3 ± 4.2 | 0.6 ± 0.3 |
| 0.94 | | | | 305.1 ± 1.3 | 311.2 ± 1.2 | 1.0 ± 0.3 |
| 0.97 | 303.1 ± 1.5 | 307.4 ± 2.1 | | 312.6 ± 0.8 | 315.9 ± 0.7 | 1.5 ± 0.4 |
| $C_{25}$ | 310.5 | | <0.3 | 319.4 | | |

[a] Temperature obtained by X-ray diffraction.

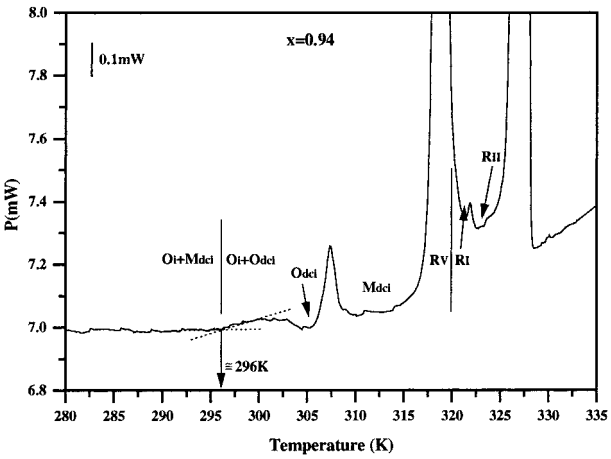


**Figure 8.** DSC thermogram of the mixed sample $(0.06)C_{23} + (0.94)C_{25}$ in rise of temperature.

Equation 15 follows from eqs 3 and 4 on substitution of eq 5 and making allowance for eq 7.

To facilitate the judgment of the results, we may recall that the leading difference property $\Delta_\alpha^\beta G_1$ follows from the "distance" from the zero line to EGC at $x = 0.5$ as

$$\Delta_\alpha^\beta G_1 = 2\{T_{EGC}(x{=}0.5) - T_{ZERO}(x{=}0.5)\}(\Delta S_A^* + \Delta S_B^*) \quad (17)$$

The information needed for eq 17, and on a wider scale for LIQFIT, is given in Table 4.

As an example from Figure 1, it can be read that for the $O_p \rightarrow R_I$ transition the EGC temperature at $x = 0.5$ is about 308 K. $T_{ZERO}$ at $x = 0.5$ is calculated as 315.0 K and, accordingly, $\Delta G_1 \approx -1900$ J mol$^{-1}$.

**Table 4. Input Data for LIQFIT Computations, Consisting of Entropies of Transition in J K$^{-1}$ mol$^{-1}$ and Temperatures of Transition in K, for Tricosane (A) and Pentacosane (B)**

| α | β | $\Delta S_A^*$ | $T_A^{\alpha\rightarrow\beta}$ | $\Delta S_B^*$ | $T_B^{\alpha\rightarrow\beta}$ |
|---|---|---|---|---|---|
| $R_{II}$ | L | 164.2 | 320.3 | 177.0 | 326.5 |
| $R_I$ | $R_{II}$ | 1.0 | 317.9 | 1.1 | 322.6 |
| $M_{dci}$ | $R_I$ | 61.4 | 312 | 70.7 | 320.0 |
| $O_p$ | $R_I$ | 61.6 | 310.7 | 71.0 | 318.8 |

**Table 5. Computed Values of the Constants (Expressed in J mol$^{-1}$) of the Excess Gibbs Energies in Eq 13**

| form i | $G_1^i$ | $G_2^i$ |
|---|---|---|
| $R_{II}$ | −100 | |
| $R_I$ | −90 | |
| $M_{dci}$ | 2620 | 1120 |
| $O_p$ | 1850 | −30 |

The complete set of excess function constants calculated by LIQFIT is given in Table 5, the complete (i.e., for the equilibria treated) phase diagram is shown in Figure 9a, and the individual $[O_p + R]$ and $[M_{dci} + R]$ loops are shown in Figure 9**,** b and c, respectively.

## Discussion

**(a) The System $C_{23} + C_{25}$ from a Phenomenological Point of View.** Our DSC and X-ray measurements have revealed a complex binary $C_{23} + C_{25}$ phase diagram, especially at low temperature. No fewer than eight phases are encountered, four at high temperature

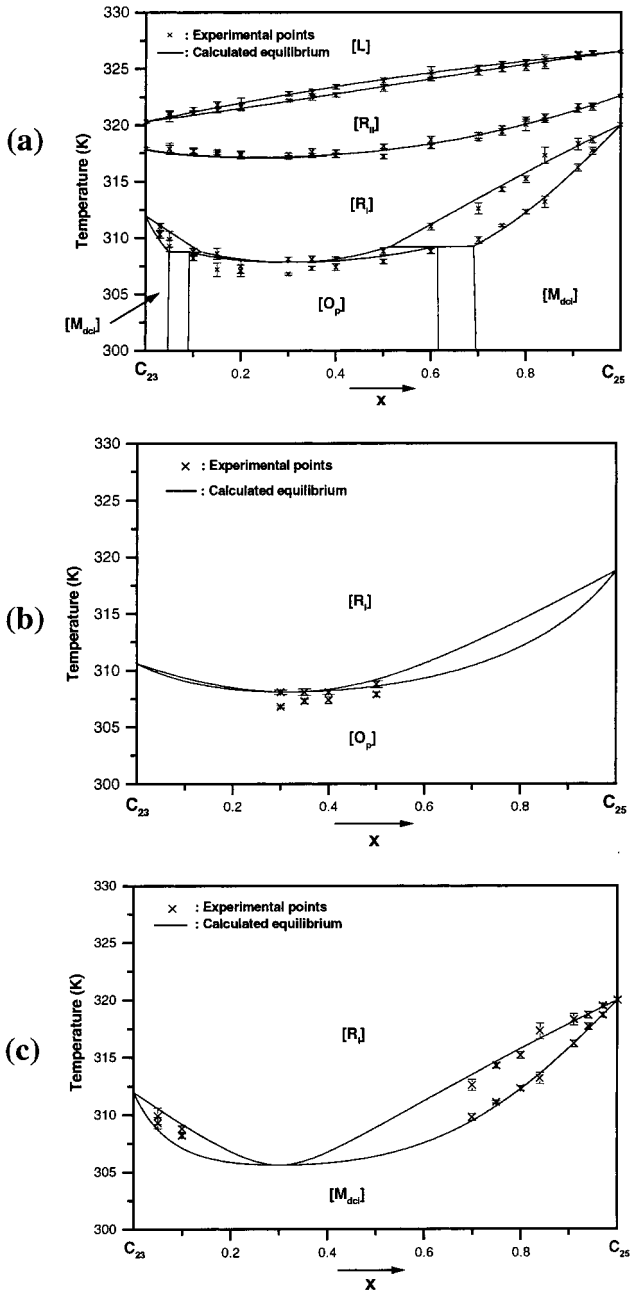


**Figure 9.** Calculated phase diagram (for the equilibria treated) along with the experimental points: (a) complete, (b) [$O_p$ + R] loop, and (c) [$M_{dci}$ + R] loop.

(the $R_{II}$, $R_I$, $R_V$, and the liquid) and four at low temperature ($O_i$, $O_{dci}$, $M_{dci}$, and $O_p$).

At high temperature, complete miscibility is observed in the three rotator phases ($R_{II}$, $R_I$, and $R_V$), the latter forms being stable for the components. At low temperature, while the $O_i$ and $O_{dci}$ forms are observed for the components, the $M_{dci}$ form is stabilized by mixing for compositions either rich in $C_{25}$ or rich in $C_{23}$. For the latter, the $M_{dci}$ form is metastable. This phase always appears in binary systems, implying at least one odd alkane (in the range $C_{16}$ to $C_{28}$), and is stabilized in the temperature × composition region close to the odd alkanes.[10]

The $O_p$ form is stabilized in the central compositional region and is metastable for both components $C_{23}$ and $C_{25}$. This form appears in all odd−odd systems (in the range $C_{16}$ to $C_{28}$) and always in the central compositional region with the exception of the $C_{25}$ + $C_{27}$ system.[10] In odd−even, even−odd, and even−even binary systems, the $O_p$ form is encountered near the $T_p$ ($C_{16}$ to $C_{24}$)[10,11,13] or $M_{011}$ ($C_{26}$ and $C_{28}$)[10] phase of the even pure alkane.

**(b) Methodology.** In this paper we outlined and applied a simple, transparent thermodynamic methodology based on (real and virtual) pure component transition properties and in terms of temperature-independent excess Gibbs energy functions. The main purpose of the methodology comes down to having a thermodynamic medium for the verification and fitting of experimental phase diagram data. Against this background some observations can be made.

First of all, the agreement between experimental data and calculated phase diagram(s) means that the system of equations and properties is consistent as far as the phase diagram is concerned. It implies, in addition, that any change in the input properties will have a direct influence on the output excess function parameters. For instance, if all transition temperatures would be raised by one degree, the result would be a change in $\Delta G_1$ of about minus 0.3 kJ $mol^{-1}$.

In the same context, the use of a uniform formula for the heat of transition as a function of chain length is justified, even and although a direct experimental proof for the $O_p$ (and also for the $M_{dcp}$ in the case of other systems than $C_{23}$ + $C_{25}$) is lacking.

As for the excess Gibbs energy, although we have used temperature-independent functions, we are aware of the fact that it rapidly changes with temperature. In forthcoming papers on *n*-alkane systems, therefore, we will make a clear distinction between the mathematical fitting of phase diagram data by means of thermodynamic formulas and the real physical nature of the mixed crystalline state. The latter aspect will be treated in a work of a global scope, comparable with our papers on the family of the rotator $R_I$ mixed crystals.[23]

CM991039+